Composites Part A 110 (2018) 70–75

Contents lists available at ScienceDirect

Composites Part A

journal homepage: www.elsevier.com/locate/compositesa

Light-actuated reversible shape memory effect of a polymer composite

Wenbing Li[a], Yanju Liu[b], Jinsong Leng[a,*]

[a] Centre for Composite Materials and Structures, Harbin Institute of Technology (HIT), No. 2 YiKuang Street, PO Box 3011, Harbin 150080, PR China
[b] Department of Astronautical Science and Mechanics, Harbin Institute of Technology (HIT), Harbin 150001, PR China

ARTICLE INFO

Keywords:
Shape memory
Light-induced
Reversible actuator

ABSTRACT

In the current study, a novel polymer composite with excellent light-actuated two-way shape memory effect (2W-SME) was fabricated using poly (ethylene-co-vinyl acetate) (EVA) as matrix and *p*-aminodiphenylimide (*p*-AP) as both light-absorber and heat source (EVA/*p*-AP). Unlike traditional thermally-driven two-way reversible shape memory polymers, in our concept, the EVA/*p*-AP featured remotely controlled and light-manipulatable reversible two-way shape memory behaviors. Utilizing the distinct light-responsive behavior of *p*-AP in the irradiation of 365 nm ultraviolet (UV) light, the EVA/*p*-AP composite exhibited excellent light-actuated reversible 2W-SME by a light-manipulated procedure. The results from this study indicated that the composite material could have greatly potential applications in soft reversible drivers.

1. Introduction

Traditional shape memory polymers (SMPs) are an exciting class of intelligent materials that can be deformed into a provisional shape and return to the initial shape under suitable stimulus [1–13]. This ability has two distinct advantages: first, traditional SMPs can exhibit a series of complex shape transformations (spiral, petal, origami and so on) in response to an external stimulus; second, the original shape can be deformed and reprogrammed multiple times. Due to these unique properties, traditional SMPs have greatly potential applications in various fields, such as aerospace field [14], biomedical devices [15], optoelectronic field [16,17], self-healing materials [18,19] and information carriers [20–22]. However, the so-called traditional SMPs with non-reversible one-way shape memory effect (1W-SME) show disadvantages when used in some fields where reversible bidirectional SME is needed.

Most recently, semi-crystalline polymers have been reported to exhibit reversible two-way SME (2W-SME), as their synthesis is easier and cheaper than liquid crystalline elastomers or other polymers [23–27]. Two strategies have been used to realize this feature. That is, under persistent external mechanical forces [28] or stress free conditions [29], the 2W-SMPs exhibit invertible changes between two shapes upon temperature variations. The actuating mechanism of 2W-SME under constant forces is that the polymer segments crystallize and elongate along the direction of constant forces below the crystallization temperature, and melting leads to segments shrinkage above the melting temperature [30]. The behavior of 2W-SME under stress free conditions results from the correlated interplay between a network formed by chemically cross-linking and a crystalline scaffold, each having the ability of encoding a unique shape. The relaxation of elongated segments upon heating is reversed by polymer crystallization along the original pathway on cooling [31]. Currently, the known reversible shape switching of 2W-SMPs is generally observed by outer direct heating and cooling cycles, and the cooling temperatures are low [26,29]. However, this characteristic of 2W-SMPs restricts their applications in some fields, such as aerospace, textile, biomedicine, and so on. To circumvent this situation, a remotely controlled and reversible 2W-SME with relatively high cooling temperature is highly desired.

Accordingly, in this study, we report reversible 2W-SME in chemically cross-linked poly (ethylene-co-vinyl acetate) (EVA) using dicumyl peroxide (DCP) as thermal initiator with *p*-aminodiphenylimide (*p*-AP) as a light-responsive source (EVA/*p*-AP) capable of transformation between two different shapes under cyclic UV light stimulation. Herein, mainly three samples with different weight ratios of *p*-AP and EVA have been fabricated to understand the light-manipulatable 2W-SME. Excitedly, the EVA/*p*-AP composite with 0.5 wt% *p*-AP exhibits excellent 2W-SME by a light-manipulated procedure. Therefore, this developed reversible 2W-SMP can be used as remotely controlled smart devices like light-manipulated self-sufficient grippers, artificial muscles, shape-switching drug delivery carriers, and so on.

2. Experimental section

2.1. Materials

Poly (ethylene-co-vinyl acetate) (EVA, 18 wt% vinyl-acetate) was

* Corresponding author.
E-mail address: lengjs@hit.edu.cn (J. Leng).

https://doi.org/10.1016/j.compositesa.2018.04.019
Received 29 January 2018; Received in revised form 28 March 2018; Accepted 16 April 2018
Available online 17 April 2018
1359-835X/

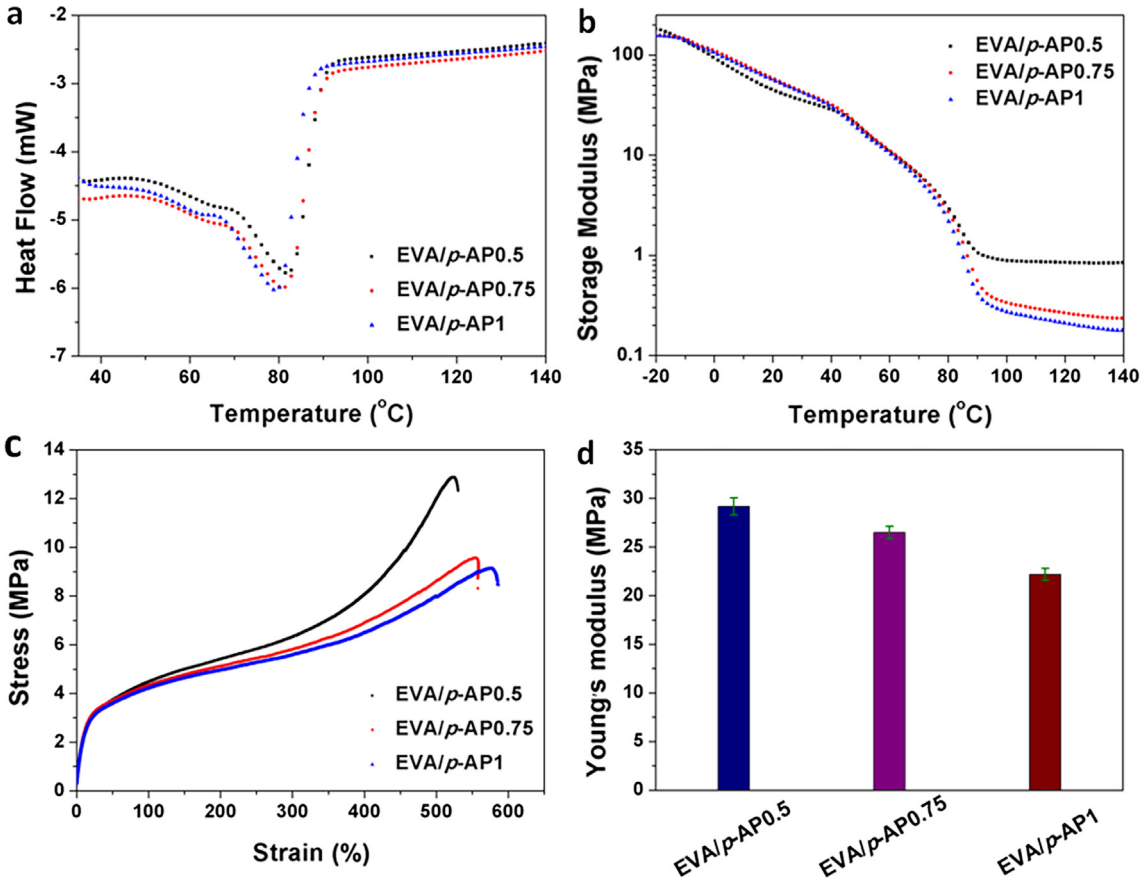

Fig. 1. (a) Representative heating DSC thermograms of the EVA/*p*-AP composites, (b) DMA curves of storage modulus, (c) tensile results at room temperature, and (d) Young's modulus values from the tensile test of the EVA/*p*-AP composites with *p*-AP: EVA weight ratios of 0.5: 100, 0.75: 100 and 1: 100. (For interpretation of the references to colour in this figure legend, the reader is referred to the web version of this article.)

purchased from DuPont Company. Dicumyl peroxide (DCP, 98%) and toluene (99.8%) were purchased from Sigma-Aldrich. The *p*-aminodiphenylimide (*p*-AP) was obtained from Aladdin. All chemical reagents were used without any further purification or modification.

2.2. Preparation

The EVA/*p*-AP polymer composite was synthesized as follows. Firstly, *p*-AP and EVA with the weight ratios of 0.5: 100, 0.75: 100 and 1: 100 were dissolved in toluene, respectively. DCP with the weight of 4% EVA was dissolved in toluene and poured into the EVA & *p*-AP mixed solutions under a high speed stirring. Secondly, the mixed solutions were volatilized in an aerator by stirring. When the mixed solutions became viscous, they were further dried in vacuum for one day at ambient temperature. After drying, the polymer mixture was thermally embossed at 130 °C for 45 min in a stainless steel mold at 3 MPa. Finally, stripping the material from the mold, the EVA/*p*-AP sheet with thickness of about 1 mm was obtained.

2.3. Characterization

Differential scanning calorimetry (DSC 1, Mettler-Toledo, Switzerland) was used to characterize the thermal properties of the polymers. Prior to the actual tests, all samples were raised to 130 °C and maintained for several minutes in order to delete any unknown thermal history. The heating rate was 10 °C min^{-1}. Dynamic mechanical analysis (DMA, Q800, TA Instruments, USA) measurements were conducted in tension mode from −30 to 150 °C. The heating rate was 3 °C min^{-1}, and the frequency was 1 Hz.

The room-temperature mechanical properties of the specimens were measured using a materials testing machine (Z010, Zwick/Roell, Germany) according to the ASTM D638 test method. The crosshead speed was 5 mm min^{-1}. Three specimens were tested.

2.4. Shape memory evaluation

DMA Q800 in a tension and controlled force mode was used to evaluate the shape memory behaviors. The rate was 5 °C min^{-1} during heating and cooling processes.

For 1 W-SME characterizations, shape fixity ratio (R_f) and shape recovery ratio (R_r) were calculated by:

$$R_f = \frac{\varepsilon}{\varepsilon_{load}} \times 100\% \quad (1)$$

$$R_r = \frac{\varepsilon - \varepsilon_{rec}}{\varepsilon} \times 100\% \quad (2)$$

ε_{load} denotes the highest strain under constraint, ε is the strain fixed after cooling and unloading, ε_{rec} is the strain which is unrecovered.

In a 2W-SME test under a constant load condition, the sample was heated at a high temperature, then a load was added. This load was kept constant in the whole testing process. The temperature was adjusted down and up between a low temperature and a high temperature at a rate of 5 °C min^{-1}.

In a 2W-SME test without stress, the samples were heated to a high temperature and kept for 5 min. Then a constant force was applied, followed by cooling the sample. When the temperature reached 0 °C, the stress was removed. Finally, shape deformation-recovery cycles were performed with repeated heating (below melting temperature) and cooling.

2.5. Macroscopic light-actuated reversible shape memory effect

Firstly, the cross-shaped sample was raised to 130 °C and kept for 5 min, deformed into a temporary shape. The temporary shape was fixed by cooling to 15 °C under outer constraint. Then the macroscopic light-actuated reversible shape memory processes were realized by an alternating UV light between on and off.

3. Results and discussion

3.1. Characterization of EVA/p-AP composites

The shape memory EVA/*p*-AP composites were fabricated in the presence of *p*-AP. The actual contents (*p*-AP: EVA) of *p*-AP were 0.5 wt %, 0.75 wt% and 1 wt%, respectively. The effects of *p*-AP contents on the thermal and thermomechanical properties of the EVA/*p*-AP composites were investigated by DSC and DMA, respectively. The melting properties of the EVA/*p*-AP composites were characterized by DSC (Fig. 1a). The melting temperatures (T_ms) were identified by the peak temperatures of the heating curves. T_m was decreased slightly from 81.8 °C to 78.7 °C as the *p*-AP content increased. The reason may be that the introduction of the *p*-AP molecules affects the crystallization behavior of the EVA, as similarly reported by Razzaq and Jacobsen [32,33].

The DSC results can characterize the thermal properties of the EVA/*p*-AP composites. However, the shape memory behaviors are closely related to their thermomechanical properties. As shown in Fig. 1b, the thermomechanical properties of the three samples were tested by DMA. The storage modulus (E') was decreased with increasing temperatures for all the samples. The E' values of the three samples were over 100 MPa at low temperatures, and then decreased to about 0.1 MPa when the temperature was over T_ms. The significant variation in E' was shown to have a great contribution to outstanding shape memory behaviors [34].

The room-temperature mechanical properties of the EVA/*p*-AP composites with different *p*-AP contents were investigated, as shown in Fig. 1c. From the stress–strain curves, the elongation at break increased with the increasing of the *p*-AP content. The composite containing 1 wt % *p*-AP (EVA/*p*-AP1) had the highest elongation at break of about 576%. The Young's moduli of the samples are shown in Fig. 1d. Both Young's modulus and tensile strength degraded gradually with the increase of *p*-AP content. This may be because of the plasticizing effect of the *p*-AP molecules. The above mechanical results indicated that introducing *p*-AP molecules changed the crystallization behavior of the EVA chains, and enhanced the ability of EVA deformation [35].

Table 1 shows the Young's moduli, tensile strengths and elongations at break of the EVA/*p*-AP composites. The elongation at break is one of the most important mechanical properties for SMPs. The elongation at break was influenced by the *p*-AP content, which increased with increasing *p*-AP content. This trend could be attributed to the *p*-AP which behaved as a plasticizer, leading to the formation of dangling chain in the EVA matrix, as similarly revealed in some papers [36,37].

3.2. One-way shape memory effect (1W-SME)

The above data (DSC, DMA, and stress–strain tests) are prepared for measuring the shape memory effects of the EVA/*p*-AP composites. The 1 W-SME of the EVA/*p*-AP specimens was studied first. Typical consecutive cycles of shape memory behaviors of the three specimens were performed using DMA, as shown in Fig. 2. The tested specimen was heated above T_m, then strained by a constant load until a temporary shape (ε_{load}). This deformed shape was fixed by cooling to low temperature followed by load release. The fixed strain was marked as ε. After maintaining at low temperature for 10 min, the specimen was heated again to recover to its initial shape. The unrecovered strain was marked as ε_{rec}. For each cycle, the values of R_f and R_r were calculated from the curves in Fig. 2 using Eqs. (1) and (2). All the specimens exhibited high R_f and R_r values (above 90%), indicating the excellent ability of the EVA/*p*-AP composites to retain the deformed shape and recover to the initial shape. However, distinct movements in the strain scopes were observed among the cycles in Fig. 2b and c. This shift could be related to the plastic flow behavior in the samples with 0.75 wt% and 1 wt% *p*-AP. The plastic flow became more and more distinct as the

Table 1
Mechanical properties of EVA/*p*-AP0.5, EVA/*p*-AP0.75 and EVA/*p*-AP1 composites.

Samples	EVA/*p*-AP0.5	EVA/*p*-AP0.75	EVA/*p*-AP1
Young's modulus (MPa)	29.16 ± 0.88	26.43 ± 0.66	22.18 ± 0.61
Tensile strength (MPa)	12.89 ± 0.39	9.56 ± 0.24	9.13 ± 0.25
Elongation at break (%)	525.97 ± 15.78	554.33 ± 13.86	575.96 ± 15.84

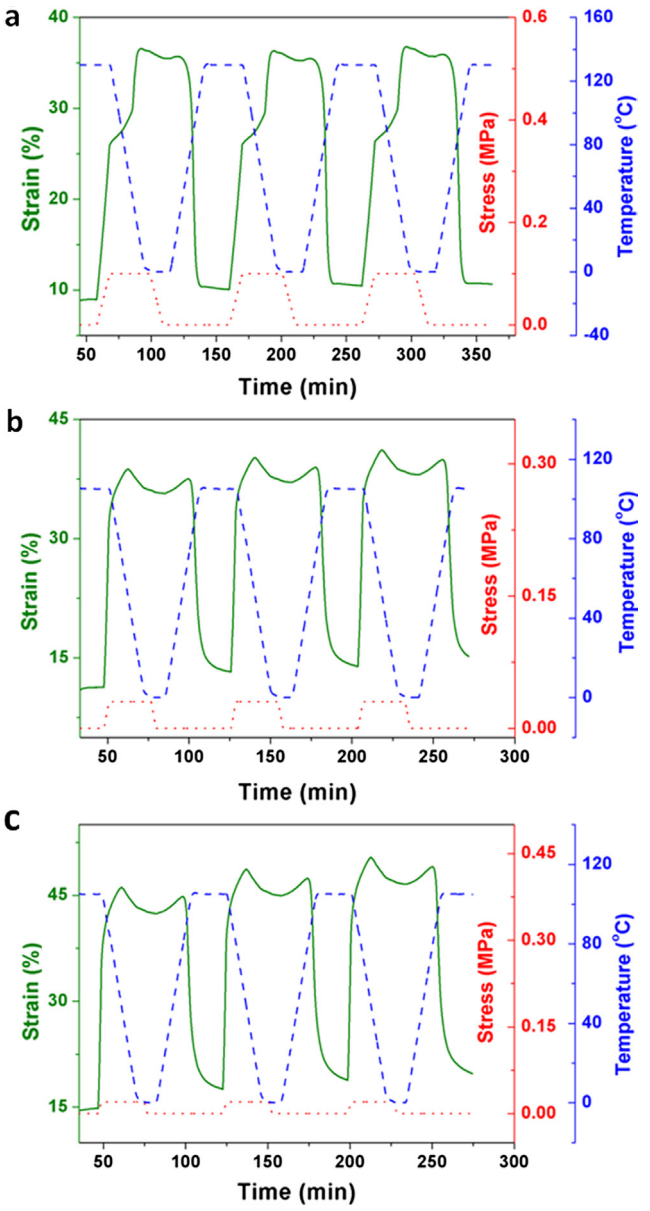

Fig. 2. Consecutive one-way shape memory cycles of EVA/*p*-AP composites: (a) EVA/*p*-AP0.5; (b) EVA/*p*-AP0.75; (c) EVA/*p*-AP1. (For interpretation of the references to colour in this figure legend, the reader is referred to the web version of this article.)

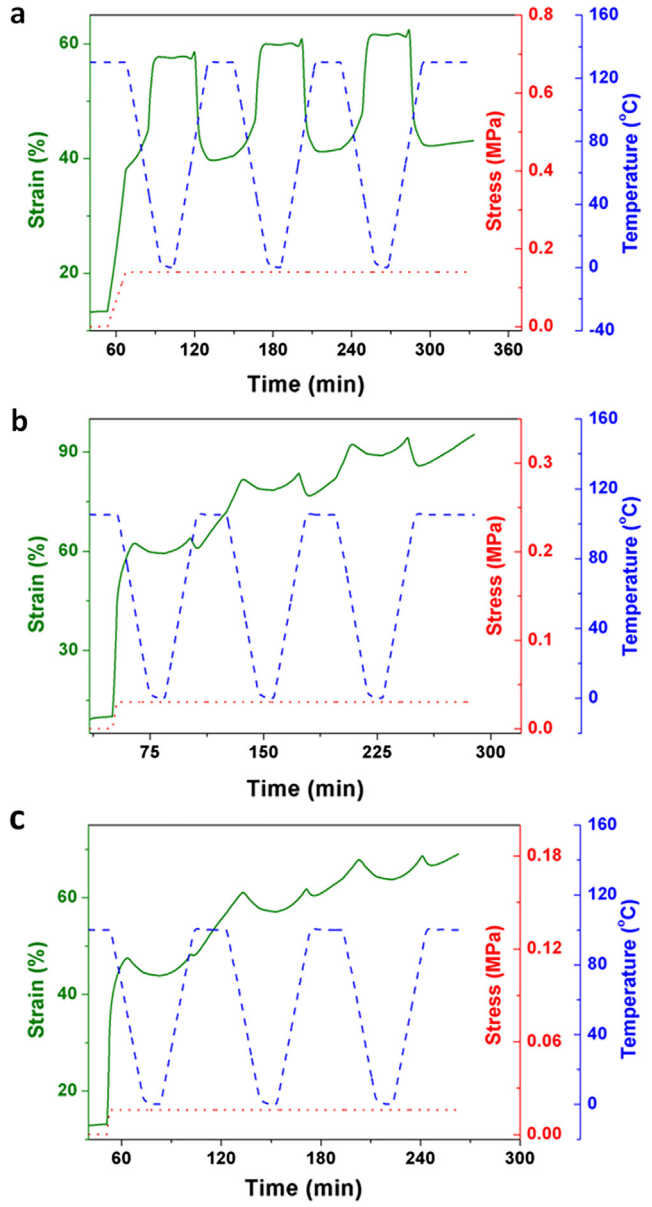

Fig. 3. Consecutive two-way shape memory cycles of EVA/*p*-AP composites under constant load conditions: (a) EVA/*p*-AP0.5; (b) EVA/*p*-AP0.75; (c) EVA/*p*-AP1. (For interpretation of the references to colour in this figure legend, the reader is referred to the web version of this article.)

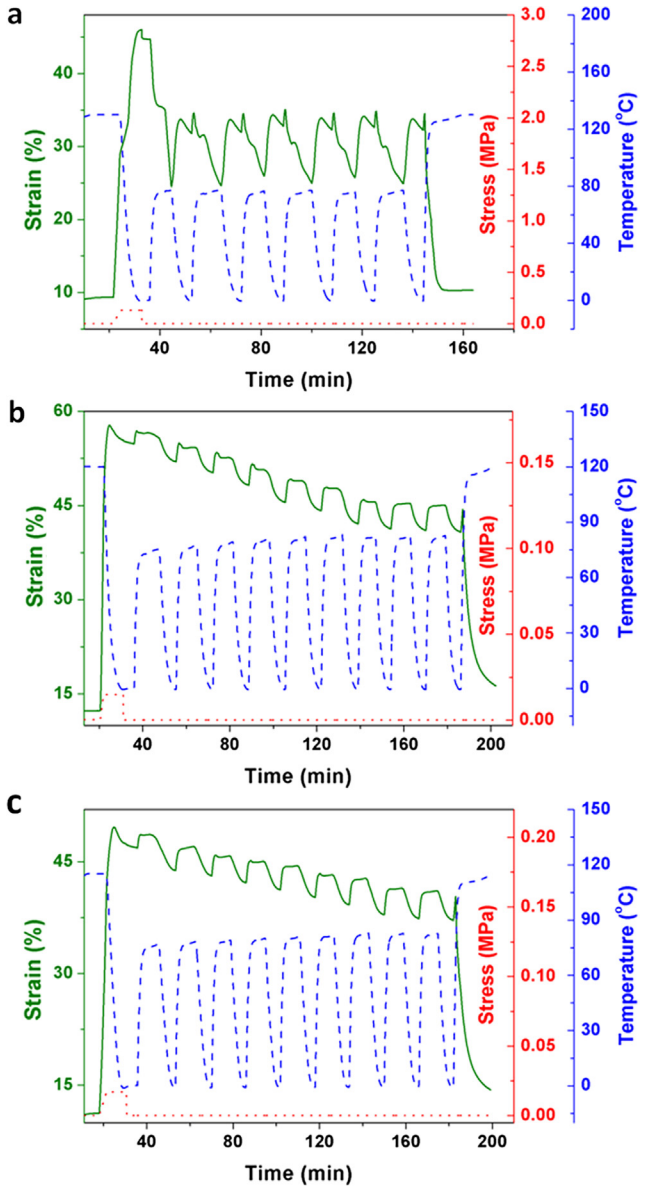

Fig. 4. Consecutive two-way shape memory cycles of EVA/*p*-AP composites under stress-free conditions: (a) EVA/*p*-AP0.5; (b) EVA/*p*-AP0.75; (c) EVA/*p*-AP1. (For interpretation of the references to colour in this figure legend, the reader is referred to the web version of this article.)

number of loading cycles increased. This may be because the plastic flow is not completely restrained by the ambient crosslinked networks [26]. However, it's worth noticing that the R_f and R_r are good in each cycle.

3.3. Two-way shape memory effect (2W-SME) under constant load conditions

It is well known that 2W-SME reveals crystallization-induced elongation (CIE) when the temperature decreases and melting-induced contraction (MIC) when the temperature increases [25]. During MIC, the segment melting leads to sample contraction due to entropy elasticity [38].

In the present study, when the samples underwent cycles of cooling and heating under a constant stress (0.14 MPa), the two-way reversible shape memory properties were revealed in Fig. 3. The two-way shape memory cycles (2W-SMC) of the specimen with 0.5 wt% *p*-AP (EVA/*p*-AP0.5) are recorded in Fig. 3a. In the 2W-SMC, the specimen is first heated above T_m and a constant load is then applied, resulting in the original strain (ε_o) at high temperature. Upon cooling, the specimen elongates, leading to the low temperature strain (ε_{low}). When heated again, the sample contracts, resulting in the recovered high temperature strain, marked as ε_{high}. The actuation strain (R_{str}) and actuation reversibility (R_{rev}) are defined as $(\varepsilon_{low} - \varepsilon_{high}) \times 100\%$ and $(\varepsilon_{low} - \varepsilon_{high}/\varepsilon_{low} - \varepsilon_o) \times 100\%$, respectively. The values of R_{str} are 18.1% (first cycle), 18.7% (second cycle) and 19.3% (third cycle). Accordingly, the R_{rev} are 95.3% for the first cycle, 88.7% for the second cycle and 84.7% for the third cycle, respectively. In addition, the ε_{low} for the three cycles is 59.7 ± 1.9%, indicating the EVA/*p*-AP0.5 specimen has 2W-SME with large reversible deformations [39].

As shown in Fig. 3b, the creep effect is observed in the three cycles rather than a CIE event, and the strain range shifts toward higher values as the cycle number increased. This phenomenon is consistent with Fig. 2b. Upon heating in each cycle, the R_{str} is quite small, and it is even more clearly noticed in Fig. 3c. This may be because the re-

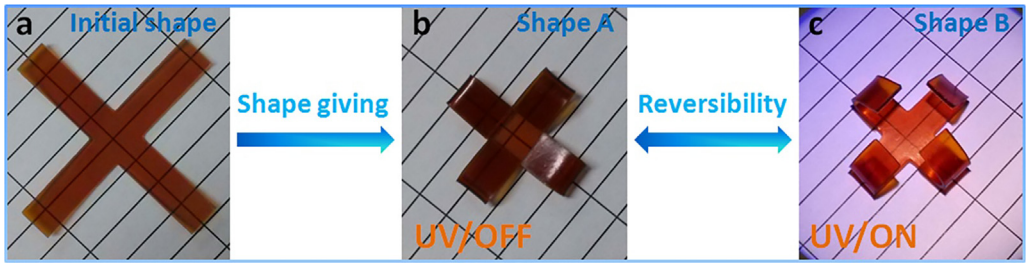

Fig. 5. Illustration of the two-way shape memory effect by UV irradiation: (a) initial cross-shaped specimen of EVA/*p*-AP0.5, (b) programmed shape, (c) gripper-like shape unfolded after UV irradiation. (For interpretation of the references to colour in this figure legend, the reader is referred to the web version of this article.)

crystallization of polymer chains did not strictly follow the orientation of the external load during cooling. After all, it is *p*-AP molecules that affect the crystallization behavior of the EVA chains [35]. Clearly, the EVA/*p*-AP0.75 and EVA/*p*-AP1 specimens do not display obvious 2W-SME despite of their fairly excellent 1 W-SME.

3.4. Two-way shape memory effect (2W-SME) under stress-free conditions

The previous section explored the 2W-SME of EVA/*p*-AP samples under constant external loads. The stress-free condition, however, is urgently required in some practical target applications. Hence, the reversible shape switch behavior of EVA/*p*-AP samples under stress-free conditions was investigated in Fig. 4. Fig. 4a gives the typical strain–stress changes *vs.* temperature of EVA/*p*-AP0.5 specimen. Firstly, the specimen was thermally equilibrated at 130 °C for 10 min. Then a stress of 0.13 MPa was loaded by 0.05 MPa min^{-1}. Secondly, the temperature was decreased to 0 °C, and the stress was unloaded. Thirdly, the temperature was kept at 0 °C for 3 min. Finally, the reversible bidirectional shape memory behaviors were achieved by repeated heating (77 °C) and cooling (0 °C).

As shown in Fig. 4a, the strain spontaneously shrinks after heating to 77 °C and elongates while re-cooling to 0 °C without any external stress. Then the specimen transformed reversibly between an extended shape and a partially recovered shape, and the reversible actuation strain was found to be stable in the latter three cycles. After six cycles, the temperature was raised to 130 °C, and the specimen recovered to its initial shape. In the course of reversible actuation, the strain shrinkage at high temperature can be attributed to partial melting of crystallization area. In addition, the unmelted region supported the structure for keeping the arrangements of polymer chains. When the temperature decreased, the amorphous networks crystallized following the orientation of the unmelted crystalline scaffold [23,31]. Therefore, the polymer was elongated and the 2W-SME was achieved. Compared to EVA/*p*-AP composites, the shape memory properties (one-way and two-way) of neat EVA matrix were shown in previous report [40], conforming that the introduction of *p*-AP (0.5 wt%) has little effect on the shape memory properties of EVA/*p*-AP0.5 composite.

As shown in Fig. 4b and c, after programming at a constant stress and stress removal, the strain thermal expansion as the temperatures raised from low temperature to high temperature and cooling shrinkage as the temperatures decreased from high temperature to low temperature was noticed in each cycle. It is a common behavior for polymers. Throughout nine heating–cooling cycles, with the increase of the cyclic number, strains of the samples (EVA/*p*-AP0.75 and EVA/*p*-AP1) tended to decrease. Clearly, the inability of EVA/*p*-AP0.75 and EVA/*p*-AP1 specimen to exhibit 2W-SME under a non-load condition was validated. Based on the contents studied above, the EVA/*p*-AP0.5 sample showed excellent cyclability and highest R_{str}, so it was selected to perform the following experiment.

Based on the light-thermal behavior of the *p*-AP [41], the macroscopical reversible shape memory cycle of EVA/*p*-AP0.5 with a light source instead of direct heating is investigated in Fig. 5. Initially, the cross-shaped sample was deformed into a gripper-like shape at 130 °C, cooled to 15 °C for shape fixation. The light-induced two-way shape memory behavior is carried out by the irradiation of 365 nm UV light where the gripper opens up to some extent (shape B) which goes back to the closed gripper-like shape (shape A) by turning off UV light. The sample reversibly switches between the two shapes (A ↔ B) on cyclic UV light stimulation, as also observed obviously from the curve of strain *vs.* time (Fig. 4a). And the sample demonstrates reproducibility in several repeating cycles. Through focusing on the macroscopical light-induced reversible shape memory behavior, we find that the EVA/*p*-AP0.5 specimen has an excellent 2W-SME when irradiated by UV light.

4. Conclusions

In this study, one type of light-induced reversible SMP based on a chemically cross-linked poly (ethylene-co-vinyl acetate) (EVA) network with *p*-aminodiphenylimide (*p*-AP) as light-absorber source (EVA/*p*-AP) was developed originally. In this system, the 2W-SME of the EVA/*p*-AP was realized due to the elongation induced by low-temperature crystallization and contraction due to high-temperature melting. In addition, the light-induced shape memory effect was achieved on account of the light-responsive behavior of the *p*-AP, which acted as light-absorber and heat source to directly convert light energy into heat. The results of the reversible actuation and light-responsive property indicated that the EVA/*p*-AP composite possessed an excellent light-induced reversible bidirectional shape memory effect. Thus, the study provides a new concept of remotely controlled and light-manipulatable shape-switching devices like self-sufficient smart devices.

Acknowledgements

This work is financially supported by the National Natural Science Foundation of China (Grant Nos. 11632005 and 11672086) and Foundation for Innovative Research Groups of the National Natural Science Foundation of China under the Grant No. 11421091, for which we are very grateful.

References

[1] Behl M, Lendlein A. Shape-memory polymers. Mater Today 2007;10(4):20–8.
[2] Xie T. Tunable polymer multi-shape memory effect. Nature 2010;464(7286):267–70.
[3] Li W, Gong T, Chen H, Wang L, Li J, Zhou S. Tuning surface micropattern features using a shape memory functional polymer. RSC Adv 2013;3(25):9865–74.
[4] Leng J, Lan X, Liu Y, Du S. Shape-memory polymers and their composites: stimulus methods and applications. Prog Mater Sci 2011;56(7):1077–135.
[5] Meng Q, Hu J. A review of shape memory polymer composites and blends. Compos Part A 2009;40(11):1661–72.
[6] Lendlein A, Jiang H, Jünger O, Langer R. Light-induced shape-memory polymers. Nature 2005;434(7035):879–82.
[7] Wu Y, Hu J, Zhang C, Han J, Wang Y, Kumar B. A facile approach to fabricate a UV/heat dual-responsive triple shape memory polymer. J Mater Chem A 2015;3(1):97–100.
[8] Habault D, Zhang H, Zhao Y. Light-triggered self-healing and shape-memory polymers. Chem Soc Rev 2013;42(17):7244–56.
[9] Liu T, Zhou T, Yao Y, Zhang F, Liu L, Liu Y, et al. Stimulus methods of multi-functional shape memory polymer nanocomposites: A review. Compos Part A 2017;100:20–30.

[10] Bai Y, Chen X. A fast water-induced shape memory polymer based on hydroxyethyl cellulose/graphene oxide composites. Compos Part A 2017;103:9–16.
[11] Fang Y, Ni Y, Choi B, Leo SY, Gao J, Ge B, et al. Chromogenic photonic crystals enabled by novel vapor-responsive shape-memory polymers. Adv Mater 2015;27(24):3696–704.
[12] Fang Y, Ni Y, Leo S, Taylor C, Basile V, Jiang P. Reconfigurable photonic crystals enabled by pressure-responsive shape-memory polymers. Nat Commun 2015;6:7416–23.
[13] Li W, Liu Y, Leng J. Selectively actuated multi-shape memory effect of a polymer multicomposite. J Mater Chem A 2015;3(48):24532–9.
[14] Liu Y, Du H, Liu L, Leng J. Shape memory polymers and their composites in aerospace applications: a review. Smart Mater Struct 2014;23(2):23001.
[15] Ward Small IV, Singhal P, Wilson TS, Maitland DJ. Biomedical applications of thermally activated shape memory polymers. J Mater Chem 2010;20(17):3356–66.
[16] Xu H, Yu C, Wang S, Malyarchuk V, Xie T, Rogers JA. Deformable, programmable, and shape-memorizing micro-optics. Adv Funct Mater 2013;23(26):3299–306.
[17] Xiao X, Qiu X, Kong D, Zhang W, Liu Y, Leng J. Optically transparent high temperature shape memory polymers. Soft Matter 2016;12(11):2894–900.
[18] Xiao X, Xie T, Cheng Y. Self-healable graphene polymer composites. J Mater Chem 2010;20(17):3508–14.
[19] Li G, Uppu N. Shape memory polymer based self-healing syntactic foam: 3-D confined thermomechanical characterization. Compos Sci Technol 2010;70(9):1419–27.
[20] Pretsch T, Ecker M, Schildhauer M, Maskos M. Switchable information carriers based on shape memory polymer. J Mater Chem 2012;22(16):7757–66.
[21] Ecker M, Pretsch T. Novel design approaches for multifunctional information carriers. RSC Adv 2014;4(87):46680–8.
[22] Li W, Liu Y, Leng J. Programmable and shape-memorizing information carriers. ACS Appl Mater Interfaces 2017;9(51):44792–8.
[23] Behl M, Kratz K, Zotzmann J, Nöchel U, Lendlein A. Reversible bidirectional shape-memory polymers. Adv Mater 2013;25(32):4466–9.
[24] Zhuo H, Hu J, Chen S. Study of the thermal properties of shape memory polyurethane nanofibrous nonwoven. J Mater Sci 2011;46(10):3464–9.
[25] Chung T, Romo-Uribe A, Mather PT. Two-way reversible shape memory in a semicrystalline network. Macromolecules 2008;41(1):184–92.
[26] Li J, Rodgers WR, Xie T. Semi-crystalline two-way shape memory elastomer. Polymer 2011;52(23):5320–5.
[27] Pandini S, Baldi F, Paderni K, Messori M, Toselli M, Pilati F, et al. One-way and two-way shape memory behaviour of semi-crystalline networks based on sol–gel cross-linked poly (ε-caprolactone). Polymer 2013;54(16):4253–65.
[28] Li W, Liu Y, Leng J. Shape memory polymer nanocomposite with multi-stimuli response and two-way reversible shape memory behavior. RSC Adv 2014;4(106):61847–54.
[29] Gong T, Zhao K, Wang W, Chen H, Wang L, Zhou S. Thermally activated reversible shape switch of polymer particles. J Mater Chem B 2014;2(39):6855–66.
[30] Razzaq MY, Behl M, Kratz K, Lendlein A. Multifunctional hybrid nanocomposites with magnetically controlled reversible shape-memory effect. Adv Mater 2013;25(40):5730–3.
[31] Zhou J, Turner SA, Brosnan SM, Li Q, Carrillo JY, Nykypanchuk D, et al. Shapeshifting: reversible shape memory in semicrystalline elastomers. Macromolecules 2014;47(5):1768–76.
[32] Razzaq MY, Behl M, Frank U, Koetz J, Szczerba W, Lendlein A. Oligo (ω-pentadecalactone) decorated magnetic nanoparticles. J Mater Chem 2012;22(18):9237–43.
[33] Jacobsen S, Fritz H. Plasticizing polylactide–the effect of different plasticizers on the mechanical properties. Polym Eng Sci 1999;39(7):1303–10.
[34] Rezanejad S, Kokabi M. Shape memory and mechanical properties of cross-linked polyethylene/clay nanocomposites. Eur Polym J 2007;43(7):2856–65.
[35] Kulinski Z, Piorkowska E. Crystallization, structure and properties of plasticized poly (L-lactide). Polymer 2005;46(23):10290–300.
[36] Ganguli S, Aglan H, Dean D. Microstructural origin of strength and toughness of epoxy nanocomposites. J Elastomers Plast 2005;37(1):19–35.
[37] Cao F, Jana SC. Nanoclay-tethered shape memory polyurethane nanocomposites. Polymer 2007;48(13):3790–800.
[38] Bothe M, Pretsch T. Two-way shape changes of a shape-memory poly (ester urethane). Macromol Chem Phys 2012;213(22):2378–85.
[39] Lu L, Li G. One-way multishape-memory effect and tunable two-way shape memory effect of ionomer poly (ethylene-co-methacrylic acid). ACS Appl Mater Interfaces 2016;8(23):14812–23.
[40] Qian C, Dong Y, Zhu Y, Fu Y. Two-way shape memory behavior of semi-crystalline elastomer under stress-free condition. Smart Mater Struct 2016;25(8):85023.
[41] Yu L, Wang Q, Sun J, Li C, Zou C, He Z, et al. Multi-shape-memory effects in a wavelength-selective multicomposite. J Mater Chem A 2015;3(26):13953–61.